Determination of the pole position of the lightest hybrid meson candidate

A. Rodas,[1,*] A. Pilloni,[2,3,†] M. Albaladejo,[2,4] C. Fernández-Ramírez,[5] A. Jackura,[6,7] V. Mathieu,[2] M. Mikhasenko,[8] J. Nys,[9] V. Pauk,[10] B. Ketzer,[8] and A. P. Szczepaniak[2,6,7]

(Joint Physics Analysis Center)

[1] *Departamento de Física Teórica, Universidad Complutense de Madrid, E-28040 Madrid, Spain*
[2] *Theory Center, Thomas Jefferson National Accelerator Facility, Newport News, VA 23606, USA*
[3] *European Centre for Theoretical Studies in Nuclear Physics and Related Areas (ECT*) and Fondazione Bruno Kessler, I-38123 Villazzano (TN), Italy*
[4] *Departamento de Física, Universidad de Murcia, E-30071 Murcia, Spain*
[5] *Instituto de Ciencias Nucleares, Universidad Nacional Autónoma de México, Ciudad de México 04510, Mexico*
[6] *Center for Exploration of Energy and Matter, Indiana University, Bloomington, IN 47403, USA*
[7] *Physics Department, Indiana University, Bloomington, IN 47405, USA*
[8] *Universität Bonn, Helmholtz-Institut für Strahlen- und Kernphysik, 53115 Bonn, Germany*
[9] *Department of Physics and Astronomy, Ghent University, Belgium*
[10] *Institut für Kernphysik & PRISMA Cluster of Excellence, Johannes Gutenberg Universität, D-55099 Mainz, Germany*

Mapping states with explicit gluonic degrees of freedom in the light sector is a challenge, and has led to controversies in the past. In particular, the experiments have reported two different hybrid candidates with spin-exotic signature, $\pi_1(1400)$ and $\pi_1(1600)$, which couple separately to $\eta\pi$ and $\eta'\pi$. This picture is not compatible with recent Lattice QCD estimates for hybrid states, nor with most phenomenological models. We consider the recent partial wave analysis of the $\eta^{(\prime)}\pi$ system by the COMPASS collaboration. We fit the extracted intensitites and phases with a coupled-channel amplitude which enforces the unitarity and analyticity of the S-matrix. We provide a robust extraction of a single exotic π_1 resonant pole, with mass and width $1564 \pm 24 \pm 86\,\text{MeV}$ and $492 \pm 54 \pm 102\,\text{MeV}$, which couples to both $\eta^{(\prime)}\pi$ channels. We find no evidence for a second exotic state. We also provide the resonance parameters of the $a_2(1320)$ and $a_2'(1700)$.

Introduction.— Explaining the structure of hadrons in terms of quarks and gluons, the fundamental building blocks of Quantum Chromodynamics (QCD), is of key importance to our understanding of strong interactions. The vast majority of observed mesons can be classified as $q\bar{q}$ bound states, although QCD should have, in principle, a much richer spectrum. Indeed, several experiments have reported resonance candidates that do not fit the valence quark model expectations [1–7]. These new experimental results, together with rapid advances in lattice gauge computations, open new fronts in studies of the fundamental aspects of QCD, such as quark confinement and mass generation. Since gluons are the mediators of the strong interaction, QCD dynamics cannot be fully understood without addressing the role of gluons in binding hadrons. The existence of states with explicit excitation of the gluon field, commonly referred to as *hybrids*, was postulated a long time ago [8–12], and has recently been supported by lattice [13–15] and phenomenological QCD studies [16–18]. In particular, a state with exotic quantum numbers $J^{PC}(I^G) = 1^{-+}(1^-)$ in the mass range $1.7 - 1.9\,\text{GeV}$ is generally accepted. The experimental determination of hybrid hadron properties –*e.g.* their masses, widths, and decay patterns– provides a unique opportunity for a systematic study of low-energy gluon dynamics. This has motivated the COMPASS spectroscopy program [19, 20] and the 12 GeV upgrade of Jefferson Lab, with experiments dedicated to hybrid photoproduction at CLAS12 and GlueX [21, 22].

The hunt for hybrid mesons is challenging, since the spectrum of particles produced in high energy collisions is dominated by nonexotic resonances. The extraction of exotic signatures

requires sophisticated partial-wave amplitude analyses. In the past, inadequate model assumptions and limited statistics resulted in several debatable results. The first reported candidate was the $\pi_1(1400)$ in the $\eta\pi$ final state [23–27]. A second state, the $\pi_1(1600)$, was claimed in the $\rho\pi$ and $\eta'\pi$ channels, with resonance parameters not compatible with the first one [28, 29]. COMPASS confirmed a peak in $\rho\pi$ and $\eta'\pi$ at around 1.6 GeV [30, 31] and an additional structure in $\eta\pi$, roughly at 1.4 GeV [32]. While the $\pi_1(1600)$ is closer to the phenomenological expectation for a hybrid, the microscopic interpretation of the $\pi_1(1400)$ is problematic. The observation of two 1^{-+} hybrids close in mass below 2 GeV is unexpected. Moreover, in the chiral limit, Bose symmetry would prevent the decay of a hybrid into $\eta\pi$ [33]. A tetraquark interpretation might be viable, and would explain why this state has eluded predictions in constituent gluon models. However, this interpretation is unfavored in the diquark-antidiquark model [34, 35], and would lead to the prediction of unobserved doubly charged and doubly strange mesons [36]. Establishing whether there exists one or two states in this mass region is thus a stringent test for the available phenomenological frameworks in the nonperturbative regime.

In [37] we performed the analysis of the $\eta\pi$ D-wave intensity. In this Letter, we extend the study to the exotic P-wave, and present results of the first coupled-channel

analysis of the $\eta^{(\prime)}\pi$ COMPASS data. We establish that a single exotic π_1 is needed and provide a robust extraction of its properties. We also determine the resonance parameters of the nonexotic $a_2(1320)$ and $a_2'(1700)$.

Description of the data.— We consider the mass independent analysis by COMPASS of $\pi p \to \eta^{(\prime)}\pi p$, with a 190 GeV pion beam [32]. We focus on the P- and D-wave intensities and their relative phase, in both channels. The published data are integrated over the range of transferred momentum squared $-t_1 \in [0.1, 1]\,\text{GeV}^2$. However, given the diffractive nature of the reaction, most of the events are produced in the forward direction, near the lower limit in $-t_1$. The $\eta^{(\prime)}\pi$ partial-wave intensities and phase differences are given in 40 MeV mass bins, from threshold up to 3 GeV. Intensities are normalized to the number of observed events corrected by the detector acceptance. The errors quoted are statistical only; systematic uncertainties or correlations were found to be negligible [38]. We thus assume all data points to be independent and normally distributed. As seen in Figs. 4(a) and 5(a) of [32], at the $\eta'\pi$ mass of 2.04 GeV there is a sharp falloff in the P-wave intensity and a sudden change, by 50°, in the phase difference between the P and the D waves. The candidate state $\pi_1(2015)$ claimed by E852 [39, 40] would be too broad to explain such an abrupt behavior and it is difficult to find a reasonable physical explanation. Unfortunately it is not possible to crosscheck this behavior with the $\eta\pi$ relative phase due to lack of data in the $1.8 - 2.0$ GeV region. Moreover, fitting these features of the P-wave drives the position of the a_2' to unphysical values. For these reasons, we fit to data up to 2 GeV only.

Recently, COMPASS has published the complete 3π partial-wave analysis [31], including the exotic 1^{-+} wave in the $\rho\pi$ final state. Although this dataset should in principle contribute to a coupled-channel analysis, the extraction of the resonance pole in this channel is hindered by the irreducible Deck process [41], which generates a peaking background in the exotic partial wave [42]. Since the Deck mechanism is not fully accounted in the COMPASS amplitude model, we do not include the 3π data in our analysis. As discussed in [37], neglecting additional channels does not affect the pole position, as long as the resonance poles are far away from threshold, which is the case studied here. On the other hand, enforcing unitarity allows us to properly implement the interference among the various resonances and the background.

Reaction model.— At high energies, peripheral production of $\pi p \to \eta^{(\prime)}\pi p$ is dominated by Pomeron ($\mathbb{P}$) exchange.

The diffractive character of the process entails factorization of the $\pi\mathbb{P} \to \eta^{(\prime)}\pi$ reaction, which for fixed t_1 resembles an ordinary helicity amplitude $a^J_{iM}(s)$, with $i = \eta^{(\prime)}\pi$ the final channel index, J and s the angular momentum and invariant mass squared of the $\eta^{(\prime)}\pi$ system, respectively, and $M \neq 0$ the Pomeron helicity in the Gottfried-Jackson frame (for more details, see [37]). In what follows, we restrict ourselves to $M = \pm 1$, which dominate the reaction and are related by parity; we thus drop the M index. The Pomeron virtuality t_1 is fixed to an effective value $t_\text{eff} = -0.1\,\text{GeV}^2$.

We parameterize the amplitudes using the coupled-channel N/D formalism [43],

$$a^J_i(s) = q^{J-1} p^J_i \sum_k n^J_k(s) \left[D^J(s)^{-1}\right]_{ki}, \qquad (1)$$

where $p_i = \lambda^{1/2}(s, m^2_{\eta^{(\prime)}}, m^2_\pi)/(2\sqrt{s})$ is the $\eta^{(\prime)}\pi$ breakup momentum, and $q = \lambda^{1/2}(s, m^2_\pi, t_\text{eff})/(2\sqrt{s})$ the π beam momentum in the $\eta^{(\prime)}\pi$ rest frame, with $\lambda(a, b, c)$ being the Källén triangular function.[1] The functions $n^J_k(s)$ incorporate process-dependent exchange interactions, *i.e.* "forces" acting between $\eta^{(\prime)}\pi$ and are smooth in the physical region. The $D^J(s)$ matrix contains cuts on the real axis above thresholds (right hand cuts), constrained by unitarity.

For the numerator $n^J_k(s)$, we use an effective expansion in Chebyshev polynomials in the variable $\omega(s) = s/(s + s_0)$, which for s_0 of the order of the hadronic scale $\simeq 1\,\text{GeV}^2$ reflects the short range nature of $\eta^{(\prime)}\pi$ production. A customary parameterization of the denominator is given by [44]

$$D^J_{ki}(s) = \left[K^J(s)^{-1}\right]_{ki} - \frac{s}{\pi}\int_{s_k}^{\infty} ds' \frac{\rho N^J_{ki}(s')}{s'(s' - s - i\epsilon)}, \qquad (2)$$

where s_k is the threshold in channel k and

$$\rho N^J_{ki}(s') = \delta_{ki} \frac{\lambda^{J+1/2}\left(s', m^2_{\eta^{(\prime)}}, m^2_\pi\right)}{\left(s' + s_L\right)^{2J+1+\alpha}} \qquad (3)$$

is an effective description of the left hand singularities in the $\eta^{(\prime)}\pi \to \eta^{(\prime)}\pi$ scattering controlled by the s_L parameter, which we initially fix at the hadronic scale $\simeq 1\,\text{GeV}^2$. Finally,

$$K^J_{ki}(s) = \sum_R \frac{g^{J,R}_k g^{J,R}_i}{m^2_R - s} + c^J_{ki} + d^J_{ki}\, s, \qquad (4)$$

with $c^J_{ki} = c^J_{ik}$ and $d^J_{ki} = d^J_{ik}$, is a standard parameterization for the K-matrix. In our reference model, we consider two K-matrix poles in the D-wave, and one single K-matrix pole in the P-wave; the numerator of

[1] We adopt the vector Pomeron model, and one unit of incoming momentum q is divided out because of the Pomeron-nucleon vertex [37].

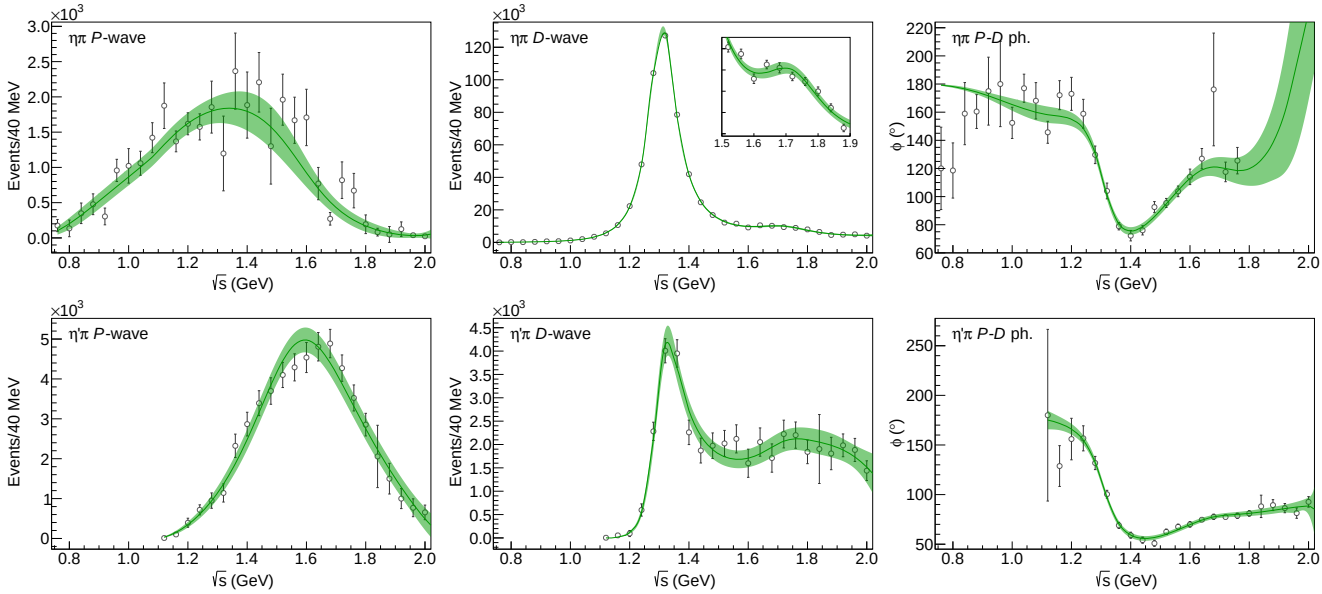

FIG. 1: Fits to the $\eta\pi$ (upper line) and $\eta'\pi$ (lower line) data from COMPASS [32]. The intensities of P- (left), D-wave (center), and their relative phase (right) are shown. The inset zooms into the region of the $a_2'(1700)$. The solid line and green band shows the result of the fit and the 2σ confidence level provided by the bootstrap analysis, respectively. The errors shown are statistical only.

each channel and wave is described by a third-order polynomial. We set $\alpha = 2$, which has been effective in describing the single-channel case [37]. The remaining 37 parameters are fitted to data, by performing a χ^2 minimization with `MINUIT` [45], and taking into account the periodicity of the phases. The initialization of the fit is chosen by randomly generating 5×10^5 different sets of values for the parameters. The best fit has $\chi^2/\text{dof} = 162/122 = 1.3$, in good agreement with data. In particular, a single K-matrix pole is able to correctly describe the P-wave peaks in the two channels at 200 MeV distance. In the $\eta\pi$ case, a conspiration between the coupled channel dynamics and the production amplitude shifts indeed the strength of the amplitude towards lower energies. The uncertainties on the parameters are estimated via the bootstrap method [46, 47]: we generate 5×10^4 pseudodata sets, and refit each one of them. The (co)variance of the parameters provides an estimate of their statistical uncertainties and correlations. The results are shown in Fig. 1, while the values of the fitted parameters and their covariance matrix are provided in the Supplemental Material [48]. The average curve passes the Gaussian test in [49].

Once the parameters are determined from the fit on the real energy axis, the amplitude can be analytically continued to complex values of s. The $D^J(s)$ matrix in Eq. (2) can be continued underneath the unitarity cut into the closest unphysical Riemann sheet. A pole s_P in the amplitude appears when the determinant of $D^J(s_P)$ vanishes. Poles close to the real axis influence the physical region and can be identified as resonances, whereas further singularities are likely to be artifacts of the specific model with no direct physical interpretation. For any practical parameterization, especially in a coupled-channel problem, it is not possible to specify *a priori* the number of poles. Appearance of spurious poles far from the physical region is thus unavoidable. It is however possible to isolate the physical poles by testing their stability against different parameterizations and data resampling.

We select the resonance poles in the $m \in [1, 2]$ GeV and $\Gamma \in [0, 1]$ GeV region, where customarily $m = \text{Re}\sqrt{s_P}$ and $\Gamma = -2\,\text{Im}\sqrt{s_P}$. We find two poles in the D-wave, identified as the $a_2(1320)$ and $a_2'(1700)$, and a single pole in the P-wave, which we call π_1. The pole positions are shown in Fig. 2, and the resonance parameters in Table I. To estimate the statistical significance of the π_1 pole, we perform fits using a pure background model for the P-wave, *i.e.* setting $g^{P,1}_{\eta^{(\prime)}\pi} = 0$ in Eq. (4). The best solution having no poles in our reference region has a χ^2 almost 50 times larger, which rejects the possibility for the P-wave peaks to be generated by some production dynamics. We also considered solutions having two isolated P-wave poles in the reference region, which would correspond to the scenario discussed in the PDG [50]. The χ^2 for this case is equivalent to the single pole solution. One of the poles is compatible with the previous determination, while the second is unstable, *i.e.* it can appear in a large region of the s-plane depending on the initial values of the fit parameters. Moreover, the behavior of the $\eta\pi$ phase required by the fit is rather peculiar.

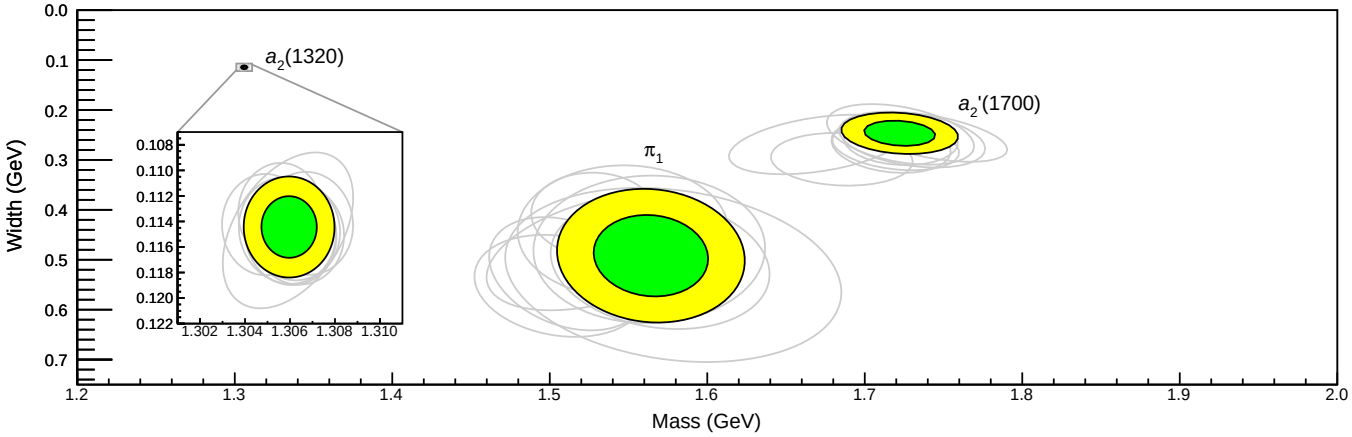

FIG. 2: Positions of the poles identified as the $a_2(1320)$, π_1, and $a_2'(1700)$. The inset shows the position of the $a_2(1320)$. The green and yellow ellipses show the 1σ and 2σ confidence levels, respectively. The gray ellipses in the background show, within 2σ, variation of the pole position upon changing the functional form and the parameters of the model, as discussed in the text

A 180° jump (due to a zero in the amplitude) appears above 1.8 GeV, where no data exist. We conclude there is no evidence for a second pole.

Systematic uncertainties.— To assess the systematic uncertainties of our results, we vary the parameters and functional forms which were kept fixed in the previous fits. We can separate these in two categories: *i*) variations which affect the smooth expansion of the numerator $n_k^J(s)$ in Eq. (1), and *ii*) variations which drive the behavior of the imaginary part of the denominator in Eq. (2). As for the latter, we study if the specific form we chose for the function $\rho N(s')$ biases the determination of the poles. We vary the value of s_L in the reference model within $[0.8, 1.8]\,\text{GeV}^2$, and reduce the value of α by one unit. Both variations alter the shape of the dispersive integral in Eq. (2), but the fit quality is unaffected. The pole positions change roughly within 2σ, as one can see in Fig. 2. The variation of α provides the largest source of systematics.

We also test a different functional form inspired by the exchange of a particle in the cross channel, $\rho N_{ki}^J(s') = \delta_{ki}\, Q_J(z_{s'})\, s'^{-\alpha}\lambda^{-1/2}(s', m_{\eta^{(\prime)}}^2, m_\pi^2)$, where $Q_J(z_{s'})$ is the second kind Legendre function, and $z_{s'} = 1 + 2s's_L/\lambda(s', m_{\eta^{(\prime)}}^2, m_\pi^2)$, with $s_L = 1\,\text{GeV}^2$. Asymptotically it behaves as $s^{-\alpha}$, has a left hand cut starting at $s = 0$, a short cut between $(s' - m_{\eta^{(\prime)}})^2$ and $(s' + m_{\eta^{(\prime)}})^2$, and an incomplete circular cut. Despite the difference in the analytic structure, it gives similar results to our reference model. We also varied $\alpha \in [1, 2]$, obtaining results similar to the model in Eq. (3) with the corresponding value of α. As for the numerator $n_k^J(s)$, we varied the effective value of the Pomeron virtuality to $t_{\text{eff}} = -0.5\,\text{GeV}^2$ and increased the order of the polynomial expansion by one unit. None of these cause important changes in pole locations. Our final estimate for the uncertainties is reported in Table I, while the detailed summary is given in the Supplemental Material [48].

TABLE I: Resonance parameters. The first error is statistical, the second systematic.

Poles	Mass (MeV)	Width (MeV)
$a_2(1320)$	$1306.0 \pm 0.8 \pm 1.3$	$114.4 \pm 1.6 \pm 0.0$
$a_2'(1700)$	$1722 \pm 15 \pm 67$	$247 \pm 17 \pm 63$
π_1	$1564 \pm 24 \pm 86$	$492 \pm 54 \pm 102$

Conclusions.— We performed the first coupled-channel analysis of the P- and D-waves in the $\eta^{(\prime)}\pi$ system measured at COMPASS [32]. We used an amplitude parameterization constrained by unitarity and analyticity. We find two poles in the D-wave, which we identify as the $a_2(1320)$ and the $a_2'(1700)$. The resonance parameters are consistent with the previous, single-channel analysis [37]. In P-wave, we find a single exotic π_1 in the region constrained by data. This determination is compatible with the existence of a single isovector hybrid meson with quantum numbers $J^{PC} = 1^{-+}$, as suggested by lattice QCD [13–15]. Its mass and width are determined to be $1564 \pm 24 \pm 86\,\text{MeV}$ and $492 \pm 54 \pm 102\,\text{MeV}$, respectively. The statistical uncertainties are estimated via the bootstrap technique, while the systematics due to model dependence are assessed by varying parameters and functional forms that are not directly constrained by unitarity. We find no evidence for a second pole that could be identified with another π_1 resonance. Solutions with two poles are possible, but do not improve the fit quality and, when present, the position of the second pole

is unstable against different starting values of the fit. It is worth noting that the two-pole solutions have a peculiar behavior of the $\eta\pi$ phase in the $\gtrsim 2\,\text{GeV}$ mass region, where no data exist.

New data from GlueX and CLAS12 experiments at Jefferson Lab in this and higher mass region will be valuable to test this behavior.

Acknowledgments.— We would like to thank the COMPASS collaboration for useful comments. AP thanks the Mainz Institute for Theoretical Physics (MITP) for its kind hospitality while this work was being completed. This work was supported by the U.S. Department of Energy under grants No. DE-AC05-06OR23177 and No. DE-FG02-87ER40365, U.S. National Science Foundation under award number PHY-1415459, Ministerio de Ciencia, Innovación y Universidades (Spain) grants No. FPA2016-75654-C2-2-P and No. FPA2016-77313-P, Universidad Complutense de Madrid predoctoral scholarship program, Research Foundation – Flanders (FWO), PAPIIT-DGAPA (UNAM, Mexico) under grants No. IA101717 and No. IA101819, CONACYT (Mexico) under grant No. 251817, the German Bundesministerium für Bildung und Forschung (BMBF), and Deutsche Forschungsgemeinschaft (DFG) through the Collaborative Research Center [The Low-Energy Frontier of the Standard Model (SFB 1044)] and the Cluster of Excellence [Precision Physics, Fundamental Interactions and Structure of Matter (PRISMA)].

* arodas@ucm.es
† pillaus@jlab.org

[1] B. Ketzer, PoS **QNP2012**, 025 (2012), arXiv:1208.5125 [hep-ex].
[2] C. A. Meyer and E. S. Swanson, Prog.Part.Nucl.Phys. **82**, 21 (2015), arXiv:1502.07276 [hep-ph].
[3] A. Esposito, A. Pilloni, and A. D. Polosa, Phys.Rept. **668**, 1 (2016), arXiv:1611.07920 [hep-ph].
[4] R. F. Lebed, R. E. Mitchell, and E. S. Swanson, Prog.Part.Nucl.Phys. **93**, 143 (2017), arXiv:1610.04528 [hep-ph].
[5] F.-K. Guo, C. Hanhart, U.-G. Meißner, Q. Wang, Q. Zhao, and B.-S. Zou, Rev.Mod.Phys. **90**, 015004 (2018), arXiv:1705.00141 [hep-ph].
[6] S. L. Olsen, T. Skwarnicki, and D. Zieminska, Rev.Mod.Phys. **90**, 015003 (2018), arXiv:1708.04012 [hep-ph].
[7] M. Karliner, J. L. Rosner, and T. Skwarnicki, Ann.Rev.Nucl.Part.Sci **68** (2018), 10.1146/annurev-nucl-101917-020902, arXiv:1711.10626 [hep-ph].
[8] D. Horn and J. Mandula, Phys.Rev. **D17**, 898 (1978).
[9] N. Isgur and J. E. Paton, Phys.Rev. **D31**, 2910 (1985).
[10] M. S. Chanowitz and S. R. Sharpe, Nucl.Phys. **B222**, 211 (1983), [Erratum: Nucl. Phys.B228,588(1983)].
[11] T. Barnes, F. Close, F. de Viron, and J. Weyers, Nucl.Phys. **B224**, 241 (1983).
[12] F. E. Close and P. R. Page, Nucl.Phys. **B443**, 233 (1995), arXiv:hep-ph/9411301 [hep-ph].
[13] P. Lacock, C. Michael, P. Boyle, and P. Rowland (UKQCD Collaboration), Phys.Lett. **B401**, 308 (1997), arXiv:hep-lat/9611011 [hep-lat].
[14] C. W. Bernard *et al.* (MILC Collaboration), Phys.Rev. **D56**, 7039 (1997), arXiv:hep-lat/9707008 [hep-lat].
[15] J. J. Dudek, R. G. Edwards, P. Guo, and C. E. Thomas (Hadron Spectrum Collaboration), Phys.Rev. **D88**, 094505 (2013), arXiv:1309.2608 [hep-lat].
[16] A. P. Szczepaniak and E. S. Swanson, Phys.Rev. **D65**, 025012 (2002), arXiv:hep-ph/0107078 [hep-ph].
[17] A. P. Szczepaniak and P. Krupinski, Phys.Rev. **D73**, 116002 (2006), arXiv:hep-ph/0604098 [hep-ph].
[18] P. Guo, A. P. Szczepaniak, G. Galata, A. Vassallo, and E. Santopinto, Phys.Rev. **D78**, 056003 (2008), arXiv:0807.2721 [hep-ph].
[19] G. Baum *et al.* (COMPASS Collaboration), (1996).
[20] P. Abbon *et al.* (COMPASS Collaboration), Nucl.Instrum.Meth. **A779**, 68 (2015), arXiv:1410.1797 [physics.ins-det].
[21] A. Rizzo (CLAS Collaboration), J.Phys.Conf.Ser. **689**, 012022 (2016).
[22] S. Dobbs (GlueX Collaboration), PoS **Hadron2017**, 047 (2018), arXiv:1712.07214 [nucl-ex].
[23] D. R. Thompson *et al.* (E852 Collaboration), Phys.Rev.Lett. **79**, 1630 (1997), arXiv:hep-ex/9705011 [hep-ex].
[24] S. U. Chung *et al.* (E852 Collaboration), Phys.Rev. **D60**, 092001 (1999), arXiv:hep-ex/9902003 [hep-ex].
[25] G. S. Adams *et al.* (E862 Collaboration), Phys.Lett. **B657**, 27 (2007), arXiv:hep-ex/0612062 [hep-ex].
[26] A. Abele *et al.* (Crystal Barrel Collaboration), Phys.Lett. **B423**, 175 (1998).
[27] A. Abele *et al.* (Crystal Barrel Collaboration), Phys.Lett. **B446**, 349 (1999).
[28] E. I. Ivanov *et al.* (E852 Collaboration), Phys.Rev.Lett. **86**, 3977 (2001), arXiv:hep-ex/0101058 [hep-ex].
[29] Yu. A. Khokhlov (VES Collaboration), Nucl.Phys. **A663**, 596 (2000), Particles and nuclei. Proceedings, 15th International Conference, PANIC '99, Uppsala, Sweden, June 10-16, 1999.
[30] M. Alekseev *et al.* (COMPASS Collaboration), Phys.Rev.Lett. **104**, 241803 (2010), arXiv:0910.5842 [hep-ex].
[31] R. Akhunzyanov *et al.* (COMPASS Collaboration), (2018), arXiv:1802.05913 [hep-ex].
[32] C. Adolph *et al.* (COMPASS Collaboration), Phys.Lett. **B740**, 303 (2015), arXiv:1408.4286 [hep-ex].
[33] F. E. Close and H. J. Lipkin, Phys.Lett. **B196**, 245 (1987).
[34] R. L. Jaffe and F. Wilczek, Phys.Rev.Lett. **91**, 232003 (2003), arXiv:hep-ph/0307341 [hep-ph].
[35] R. Jaffe, Phys.Rept. **409**, 1 (2005), arXiv:hep-ph/0409065 [hep-ph].
[36] S. U. Chung, E. Klempt, and J. G. Korner, Eur.Phys.J. **A15**, 539 (2002), arXiv:hep-ph/0211100 [hep-ph].
[37] A. Jackura *et al.* (COMPASS and JPAC Collaboration), Phys.Lett. **B779**, 464–472 (2017), arXiv:1707.02848 [hep-ph].
[38] T. Schlüter, *The $\pi^-\eta$ and $\pi^-\eta'$ Systems in Exclusive 190 GeV π^-p Reactions at COMPASS*, Ph.D. thesis, Munich U. (2012).
[39] J. Kuhn *et al.* (E852 Collaboration), Phys.Lett. **B595**,

109 (2004), arXiv:hep-ex/0401004 [hep-ex].
[40] M. Lu *et al.* (E852 Collaboration), Phys.Rev.Lett. **94**, 032002 (2005), arXiv:hep-ex/0405044 [hep-ex].
[41] R. T. Deck, Phys.Rev.Lett. **13**, 169 (1964).
[42] D. Ryabchikov, Talk at PWA9/ATHOS4, NoStop
[43] J. D. Bjorken, Phys.Rev.Lett. **4**, 473 (1960).
[44] I. J. R. Aitchison, Nucl.Phys. **A189**, 417 (1972).
[45] F. James and M. Roos, Comput.Phys.Commun. **10**, 343 (1975).
[46] W. H. Press, S. A. Teukolsky, W. T. Vetterling, and B. P. Flannery, *Numerical Recipes 3rd Edition: The Art of Scientific Computing*, 3rd ed. (Cambridge University Press, New York, NY, USA, 2007).
[47] B. Efron and R. Tibshirani, *An Introduction to the Bootstrap*, Chapman & Hall/CRC Monographs on Statistics & Applied Probability (Taylor & Francis, 1994).
[48] "Supplemental material," Also on http://www.indiana.edu/~jpac.
[49] R. Navarro Pérez, E. Ruiz Arriola, and J. Ruiz de Elvira, Phys.Rev. **D91**, 074014 (2015), arXiv:1502.03361 [hep-ph].
[50] M. Tanabashi *et al.* (Particle Data Group Collaboration), Phys.Rev. **D98**, 030001 (2018).

SUPPLEMENTAL MATERIAL

TABLE II: Parameters of the numerator $n_k^J(s) = \sum_{n=0}^{3} a_n^{J,k} T_n\left[\omega(s)\right]$. All numbers are expressed in GeV units. The first values are obtained from the best fit, and should be used to reproduce the plots. The second values contains the mean value and standard deviation estimated with bootstrap. We remark that the coefficients are 100% correlated, and the single error has to be taken with care.

	$\eta\pi$ channel			$\eta'\pi$ channel	
$a_0^{P,\eta\pi}$	409	356 ± 334	$a_0^{P,\eta'\pi}$	-47	-43 ± 39
$a_1^{P,\eta\pi}$	-633	-547 ± 534	$a_1^{P,\eta'\pi}$	66	59 ± 63
$a_2^{P,\eta\pi}$	281	240 ± 255	$a_2^{P,\eta'\pi}$	-21	-17 ± 30
$a_3^{P,\eta\pi}$	-58	-47 ± 63	$a_3^{P,\eta'\pi}$	1	-0 ± 8
$a_0^{D,\eta\pi}$	-248	-247 ± 28	$a_0^{D,\eta'\pi}$	231	233 ± 79
$a_1^{D,\eta\pi}$	414	415 ± 39	$a_1^{D,\eta'\pi}$	-291	-290 ± 125
$a_2^{D,\eta\pi}$	-191	-192 ± 39	$a_2^{D,\eta'\pi}$	177	177 ± 83
$a_3^{D,\eta\pi}$	59	61 ± 29	$a_3^{D,\eta'\pi}$	-4	-1 ± 62

TABLE III: Parameters of $D^J(s)$. The errors and correlations are estimated with bootstrap.

	Resonating terms			K-matrix background	
$g_{\eta\pi}^{P,1}$	-0.68	-0.55 ± 0.38	$c^P_{\eta\pi,\eta\pi}$	-15.43	-14.77 ± 7.22
$g_{\eta'\pi}^{P,1}$	-13.12	-13.12 ± 0.95	$c^P_{\eta\pi,\eta'\pi}$	-67.22	-65.28 ± 13.91
$m^2_{P,1}$	3.52	3.52 ± 0.08	$c^P_{\eta'\pi,\eta'\pi}$	-190.73	-184.19 ± 38.21
			$d^P_{\eta\pi,\eta\pi}$	1.82	1.93 ± 2.24
			$d^P_{\eta\pi,\eta'\pi}$	7.64	7.59 ± 5.09
			$d^P_{\eta'\pi,\eta'\pi}$	63.85	60.54 ± 18.59
$g_{\eta\pi}^{D,1}$	5.63	5.64 ± 0.34	$c^D_{\eta\pi,\eta\pi}$	-2402.56	-2385.05 ± 273.87
$g_{\eta'\pi}^{D,1}$	-3.77	-3.78 ± 0.10	$c^D_{\eta\pi,\eta'\pi}$	462.60	469.55 ± 55.87
$m^2_{D,1}$	1.86	1.86 ± 0.02	$c^D_{\eta'\pi,\eta'\pi}$	-86.60	-92.25 ± 28.11
$g_{\eta\pi}^{D,2}$	147.79	147.17 ± 9.88	$d^D_{\eta\pi,\eta\pi}$	-614.58	-608.35 ± 49.32
$g_{\eta'\pi}^{D,2}$	-33.39	-34.07 ± 3.41	$d^D_{\eta\pi,\eta'\pi}$	164.72	166.85 ± 17.46
$m^2_{D,2}$	8.06	8.06 ± 0.30	$d^D_{\eta'\pi,\eta'\pi}$	-42.19	-44.45 ± 11.59

TABLE IV: Summary of systematic studies. For each systematic variation, 5×10^4 bootstrapped pseudodatasets are produced, and the average is shown here. For each parameter varied, we consider the maximum deviation of the pole position from the one in the reference fit. If that is compatible with the statistical uncertainty, we neglect the effect. If larger, we assign a systematic uncertainty to it, and eventually add in quadrature all the systematic uncertainties.

Systematic	Poles	Mass (MeV)	Deviation (MeV)	Width (MeV)	Deviation (MeV)
Variation of the function $\rho N(s')$					
$s_L = 0.8\,\mathrm{GeV}^2$	$a_2(1320)$	1306.4	0.4	115.0	0.6
	$a_2'(1700)$	1720	−3	272	26
	π_1	1532	−33	484	−8
$s_L = 1.8\,\mathrm{GeV}^2$	$a_2(1320)$	1305.6	−0.4	113.2	−1.2
	$a_2'(1700)$	1743	21	254	7
	π_1	1528	−36	410	−82
Systematic assigned	$a_2(1320)$		0.0		0.0
	$a_2'(1700)$		21		26
	π_1		36		82
$\alpha = 1$	$a_2(1320)$	1305.9	−0.1	114.7	0.3
	$a_2'(1700)$	1685	−37	299	52
	π_1	1506	−58	552	60
Systematic assigned	$a_2(1320)$		0.0		0.0
	$a_2'(1700)$		37		52
	π_1		58		60
$Q_J, \alpha = 1$	$a_2(1320)$	1304.9	−1.1	114.2	−0.2
	$a_2'(1700)$	1670	−52	269	22
	π_1	1511	−53	528	36
$Q_J, \alpha = 1.5$	$a_2(1320)$	1306.0	0.1	115.0	0.6
	$a_2'(1700)$	1717	−5	272	25
	π_1	1578	14	530	39
$Q_J, \alpha = 2$	$a_2(1320)$	1306.2	0.2	114.7	0.3
	$a_2'(1700)$	1723	1	261	15
	π_1	1570	6	508	16
Systematic assigned	$a_2(1320)$		1.1		0.0
	$a_2'(1700)$		52		25
	π_1		53		0
Variation of the numerator function $n(s)$					
Polynomial expansion	$a_2(1320)$	1305.9	−0.1	114.7	0.3
	$a_2'(1700)$	1723	1	249	2
	π_1	1563	−1	479	−13
Systematic assigned	$a_2(1320)$		0.0		0.0
	$a_2'(1700)$		0		0
	π_1		0		0
$t_{\mathrm{eff}} = -0.5\,\mathrm{GeV}^2$	$a_2(1320)$	1306.8	0.8	114.1	−0.3
	$a_2'(1700)$	1730	8	259	13
	π_1	1546	−18	443	−49
Systematic assigned	$a_2(1320)$		0.8		0.0
	$a_2'(1700)$		0		0
	π_1		0		0